Int J. Multiphase Flow Vol 18, No. 1, pp. 41–50, 1992
Printed in Great Britain.

0301-9322/92 $5.00 + 0.00

PRESSURE DISTRIBUTION AND VORTICAL STRUCTURE IN THE WAKE BEHIND GAS BUBBLES IN LIQUID AND LIQUID–SOLID SYSTEMS

K. RAGHUNATHAN, S. KUMAR and L.-S. FAN†
Department of Chemical Engineering, The Ohio State University, Columbus, OH 43210, U.S.A.

(Received 29 January 1991; in revised form 1 August 1991)

Abstract—An important characteristic of large bubbles rising in liquid columns and liquid–solid fluidized beds is the near wake. Unsteady wakes are typified by the stable liquid layer, and the cyclic sequence of formation, growth and shedding of vortices near the bubble base. The pressure distribution in the near wake is a critical variable which determines the fluid motion, solids concentration and size of the wake, and is closely related to the wake structure. The static pressure traces in the near wake are examined with varying vertical distance from the bubble nose and lateral distance from the bubble axis of symmetry. Single bubbles are injected into a two-dimensional liquid column and a liquid–solid fluidized bed, and static pressure is measured by means of a transducer mounted on the column wall and interfaced with a high-speed computer data acquisition system. The bubble-wake is visualized using a video camera system synchronized with the data acquisition system. The geometry of the primary wake is shown to be uniquely characterized by the pressure trace, and a one-to-one correspondence between the pressure distribution and vortical structure is established. The effects of particle size and solids holdup are investigated, and compared with stationary water. Pressures vs time traces are normalized as modified pressure coefficient vs dimensionless time. These traces exhibit similar trends in stationary water and in a liquid–solid fluidized bed. However, results show that the presence of solids affects the quantitative nature of the pressure distribution in the near wake behind the bubble.

Key Words: pressure distribution, bubble-wake, liquid and liquid–solid systems

INTRODUCTION

Bubble phenomena are characteristic of multiphase contacting devices such as gas–liquid bubble columns, gas–solid fluidized beds, gas–slurry bubble columns, gas–liquid–solid fluidized beds and gas–slurry–solid fluidized beds. The fluid dynamics of these systems, which have strong effects on the mass and heat transfer and solids mixing behavior, are extremely complex and poorly understood. The wake, which resides immediately behind a rising bubble and contains a certain proportion of fluid and sometimes solids, plays a significant role in the fluid dynamics of such multiphase systems (Fan & Tsuchiya 1990). Thus, a fundamental understanding of the behavior of the wake forms the necessary basis for a complete description of the overall system performance.

Tsuchiya & Fan (1988) provided qualitative descriptions of boundaries between primary and secondary wakes in a two-dimensional projection for several important representative wake structures. For steady flows, the primary wake observed for large bubbles in a viscous medium at low Reynolds numbers (Re) is laminar and closed, and the shape and size of the boundary are invariant with time. At higher Re the wake flow is unsteady but has steady vortex shedding; the shape and size of the primary wake vary periodically. For very large bubbles at high Re the wake flow becomes unsteady with parallel wake shedding.

Pressure distribution in the wake is a critical property which is closely associated with the fluid motion, solids concentration and size of the wake, or more generally, the wake structure. Lazarek & Littman (1974) studied the pressure field around a large circular-cap bubble in water and verified the Davies and Taylor boundary condition along the bubble roof. Bessler & Littman (1987) later extended this study for liquids of different viscosities. The pressure trace showed a symmetric minimum in the primary wake; they also observed a sharp minimum followed by localized recovery of the pressure immediately beneath the bubble base, but only for low viscosities. In their investigations the bubble-wake, even for water, was closed laminar in structure, in spite of the large

†Author for correspondence.

bubble size (up to 10 cm wide). A possible cause of the closed laminar wake was the delayed onset of shedding of wall-stabilized large bubbles.

While much progress has been made in the understanding of wake phenomena, the pressure distribution in the wake in a liquid–solid system remains unexplored (Fan & Tsuchiya 1990). In this work, the wake structure and the pressure in the wake behind a circular-cap bubble in a liquid as well as in liquid–solid systems are investigated. The study is intended to establish the relationship between the pressure distribution and the vortical structure in the primary wake. With this understanding, information about the size of the stable liquid layer and the primary wake in liquid–solid suspensions can be obtained.

EXPERIMENTAL

A schematic diagram of the experimental setup is shown in figure 1. The experiments are performed in a two-dimensional Plexiglas column, 104 cm high, 40.6 cm wide and with 0.8 cm nominal gap thickness. The liquid enters the column through four inlet valves and four

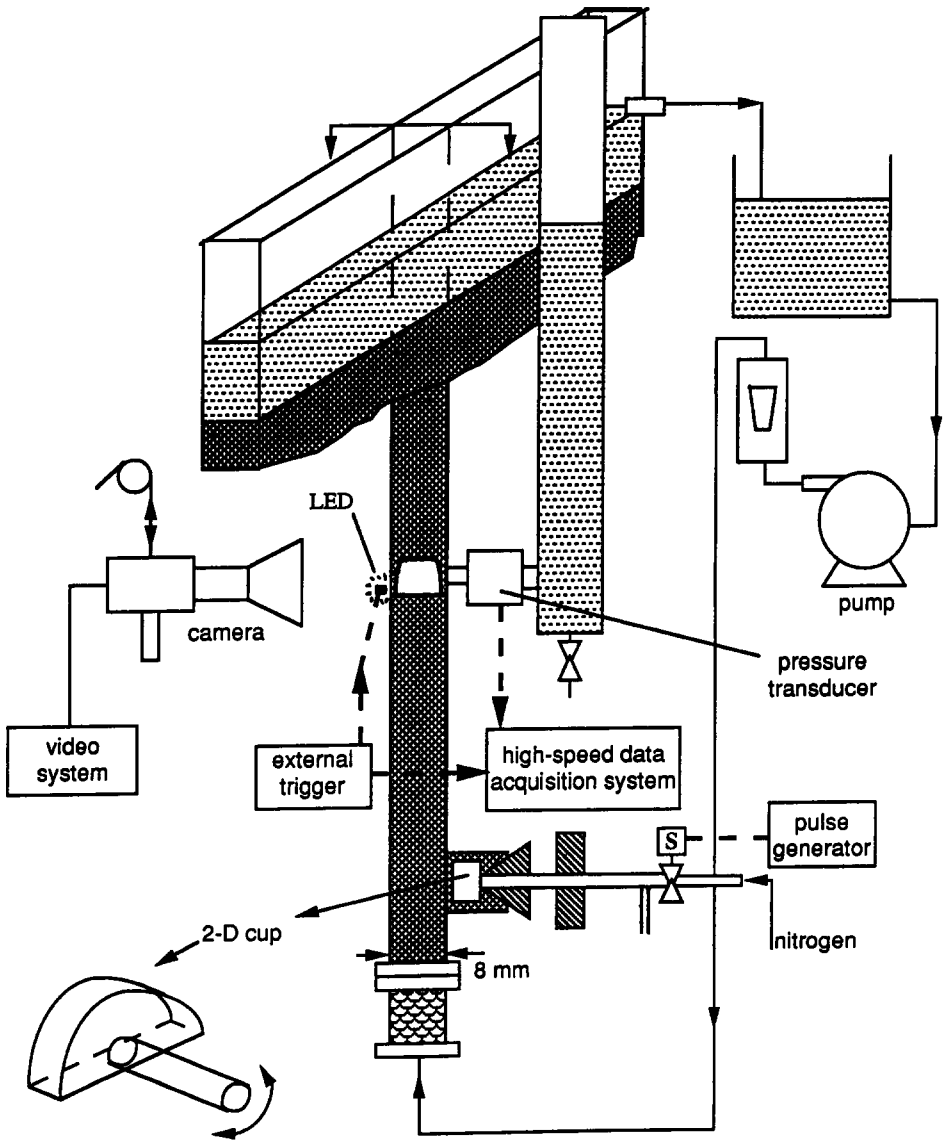

Figure 1. Schematic diagram of the experimental setup

compartments, each 12.7 cm high, and a packed bed of two layers: 3 mm lead shot and 774 μm glass beads. The support for the fluidized particles is provided by 200-mesh wire cloth. A constant liquid velocity is maintained by circulating water through a reservoir and a rotary pump.

Common methods for single bubble injection employed in the literature involve the use of a solenoid valve or trapping of the bubble in a cup and then releasing it. While the solenoid valve injection transmits a shock which interferes with the pressure signals, the presence of a cup in the column directly below the probe disturbs the fluidized state, and hence the bubble-wake behavior, in a liquid–solid system. A two-dimensional cup bubble injection system is designed in this study to circumvent these problems: two semi-circular disks of 3.8 cm dia are set 6 mm apart by a semi-circular ring. One end of a 0.64 cm tube is inserted into one of the disks and the other end is connected to a gas line through a solenoid valve. To prevent local non-uniformity in the bed, this cup is housed within a circular recess in the rear wall of the column, as shown in figure 1. The bubble is injected into the cup through the solenoid valve and the trapped bubble is then released by turning the cup. The cup is reinforced at the tube to prevent any lateral motion during bubble release. With this bubble injection system, disturbance in the pressure signal and the wake behavior is kept minimal.

A probe is flush mounted at the rear wall of the column and is connected to the positive end of a differential pressure transducer (Validyne, DP-15). The probe is located at about 70 cm from the point of bubble injection, which allows sufficient distance for the bubble to reach its terminal velocity. The negative end of the transducer is connected to a liquid column to offset the static pressure head in the experimental column above the probe. Thus, the pressure signals obtained correspond to the differential pressure due to the passage of the bubble and the wake. The pressure transducer is interfaced with a high-speed microcomputer data acquisition system. Pressure signals are sampled at the rate of 250 points/s. Digitized signals stored in the computer are later converted to pressure values via the transducer calibration. A typical signal recorded by the data acquisition system is shown in figure 2. Note that the bubble was released after the data acquisition was started. It is clear that the disturbance due to bubble release is negligible.

For typical signals in stationary water, the pressure values range between -10 and 5 mmH_2O. If a solenoid valve is used directly without the recessed cup, the disturbance due to bubble injection exceeds the detection range of the data acquisition system (-25 to 25 mmH_2O) initially, and then dampens off gradually. The amplitude of these fluctuations, when the bubble reaches the probe, is comparable in magnitude to the first maximum in the pressure signals.

Visualization of the bubble-wake is performed in the freeboard region of a 163 μm bed, with the entrained particles serving as tracers. The wake structure is observed by a video camera (Pulnix)

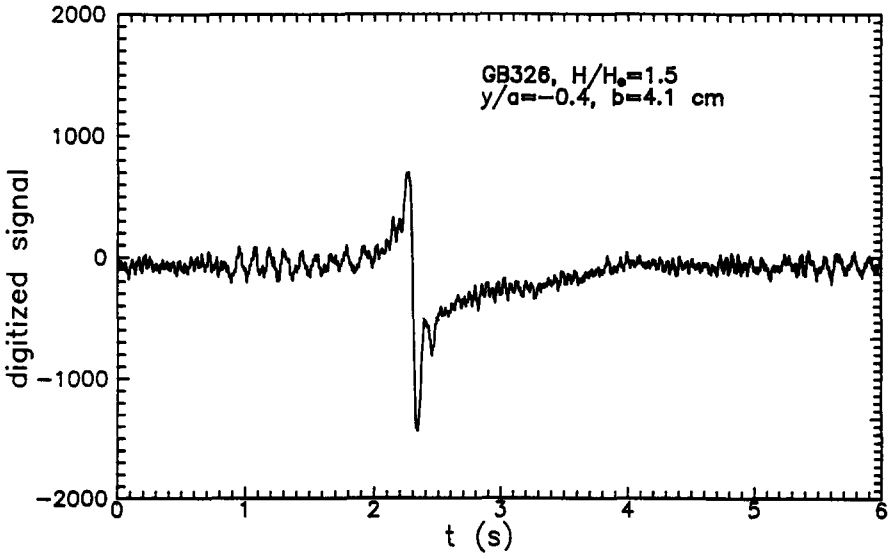

Figure 2. Raw signal recorded by the data acquisition system.

which is moved at the same speed as the rising bubble by a pulley mechanism. The signals from the camera are stored by a video recorder (Sony VO-5800 U-matic) at a rate of 60 frames/s.

A light-emitting diode (LED) is located in the front wall of the column in the view of the video camera. An external trigger activates the data acquisition system and illuminates the LED simultaneously. Thus, precise synchronization of the video and pressure signals is achieved.

Pressure signals were obtained for bubbles rising in stationary tapwater and in a liquid–solid fluidized bed of particles of two different sizes at bed expansion ratios (H/H_0) of 1.5 and 2.0. The physical properties of the solid particles are given in table 1. In most of the experiments, the bubble width was about 4 cm with an absolute rise velocity of about 29 cm/s which corresponds to an Re value of about 11,000, based on the bubble width and liquid properties. At the Re values used in our experiments, the bubble is circular-cap shaped and the near wake has an open structure with shedding vortices.

RESULTS AND DISCUSSION

In order to compare the signals for different cases, the time and pressure values are reduced to the dimensionless forms τ and pressure coefficient C_p, respectively, where

$$\tau = U_b t/a \qquad [1]$$

and

$$C_p = (p - p_\infty)/(\tfrac{1}{2}\rho_m U_b^2). \qquad [2]$$

In the above equations a is the half bubble width and $(p - p_\infty)$ is the differential pressure, p_∞ being the baseline pressure; ρ_m and U_b are the mixture density and relative rise velocity of the bubble, respectively. For liquid–solid systems, as proposed by El-Temtamy & Epstein (1980),

$$\rho_m = \rho_s \epsilon_s + \rho_L(1 - \epsilon_s) \qquad [3]$$

and

$$U_b = U_b' - U_L/(1 - \epsilon_s), \qquad [4]$$

where ρ_s is the solids density, ρ_L is the liquid density, ϵ_s is the solids holdup, U_b' is the absolute bubble rise velocity (relative to stationary coordinates) and U_L is the liquid velocity. The absolute bubble rise velocity is determined using the video system by measuring the number of frames (and hence the time) elapsed as the bubble traverses two fixed locations along the column at 63 and 78 cm from bubble injection. Note that ρ_m and U_b reduce to ρ_L and U_b', respectively, for the case of stationary water.

A frame-by-frame analysis of video signals is performed in conjunction with the pressure–time traces to establish the relationship between the vortical structure and pressure distribution in the bubble-wake. A representative pressure signal and selected photographs of the vortical structure corresponding to this signal are shown in figure 3. In this figure and in all the pressure signals shown in this paper, the zero of the abscissa corresponds to the horizontal plane in which the bubble nose lies; b is the bubble width, $a = b/2$ and y is the lateral displacement from the bubble axis of symmetry. In the photographs, the black dot or the tip of the arrow indicates the location of the pressure probe. In this run, the probe senses the pressure across the vortex attached to the rising bubble. While the first maximum (τ_0, C_{p0}) in the pressure trace lies in the frontal field of the bubble, the first minimun (τ_1, C_{p1}) is located just beneath the bubble base within the stable liquid layer region defined by Tsuchiya & Fan (1988). The second maximum (τ_2, C_{p2}) is at the boundary

Table 1. Physical properties of spherical particles

Particle	Notation	Average dia (mm)	Density (g/cm^3)	ϵ_{s0}^*
Glass bead	GB163	0.163	2.50	0.63
Glass bead	GB326	0.326	2.50	0.62

*Packed bed solids fraction.

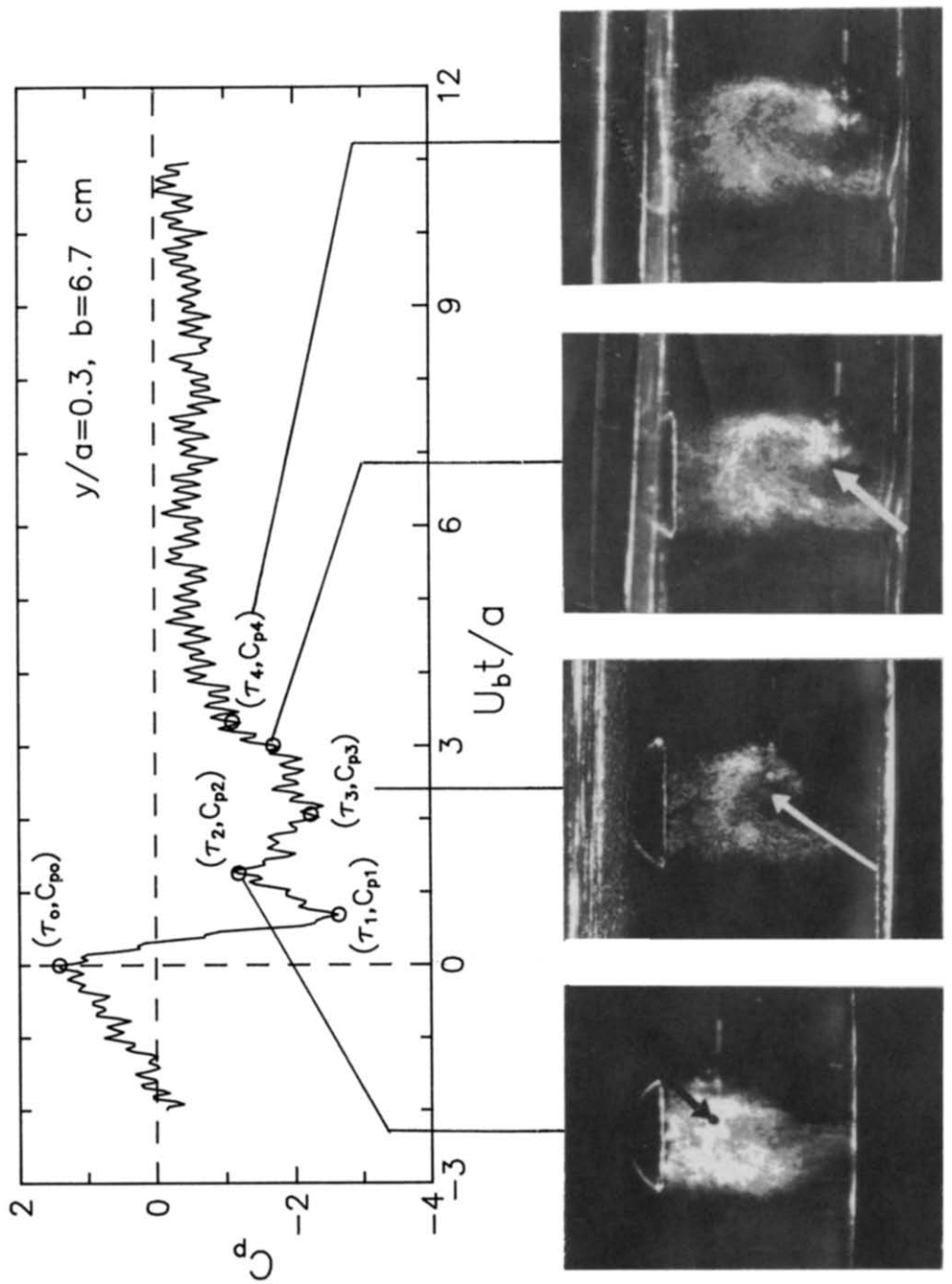

Figure 3 Relationship between the vortical structure and the pressure signal Visualization performed in the freeboard region of a 163 μm bed, with the entrained particles serving as tracers

between the stable liquid layer and the vortex and thus it corresponds to the beginning of the circulatory region. The second minimum, located near (τ_3, C_{p3}), is in the horizontal plane in which the vortex center lies, and this concave region is not as sharp as the first minimum. Tsuchiya & Fan (1988) defined the boundary of the primary wake as the cut-off stream flowing across the wake and the end of the concave region, located at (τ_4, C_{p4}) in the pressure signal, is at the cut-off stream as shown by the photograph. Similar results are obtained for several other runs where the visualization was coupled with pressure traces. The first minimum is very close to the bubble base. Thus, the regions corresponding to $(\tau_2 - \tau_1)$, $(\tau_4 - \tau_2)$ and $(\tau_4 - \tau_1)$ measure the sizes of the stable liquid layer, the vortex and the primary wake, respectively.

Figures 4(a, b) compare two signals which were analyzed in conjunction with the video pictures, although the photographs for these cases are not shown here. In both the signals, the second vertical dashed line corresponds to the horizontal plane in which the bubble base lies. For figure 4(a), the probe cuts across the vortex, similar to that shown in figure 3. The corresponding pressure signal shows a pronounced and symmetric concave region about the vortex center; the magnitude of the pressure at this location is large and the pressure recovery is sharp. Figure 4(b), on the other hand, corresponds to the case where the probe was located outside the visible boundary of the vortex. The second minimum in this case is still located in the same horizontal plane as the vortex center; however, its magnitude is less than that in figure 4(a) and the pressure recovery is also not as sharp. The location of (τ_4, C_{p4}) cannot be identified easily for this signal. These two signals show that a symmetric concave region can be observed only along a vertical axis passing through the vortex.

Pressure traces along a vertical axis passing through the bubble nose ($y/a = 0$) in stationary water are shown in figure 5. For a bubble rising in stationary water it can be assumed that the flow field in front of the bubble is irrotational and hence Bernoulli's theorem with respect to a moving coordinate located at the bubble nose is valid. For this case the value of C_p at the nose of the bubble should be unity. In figure 5 the pressure coefficient at the nose of the bubble approaches unity, but in some cases this value is somewhat less than one. This can be attributed to the slight three-dimensional effect in the column and/or bubble rocking. The concave region in the case of stationary water is relatively pronounced indicating the presence of a prominent vortex. Following this, the pressure approaches the free stream value. However, the presence of the secondary wake results in incomplete pressure recovery.

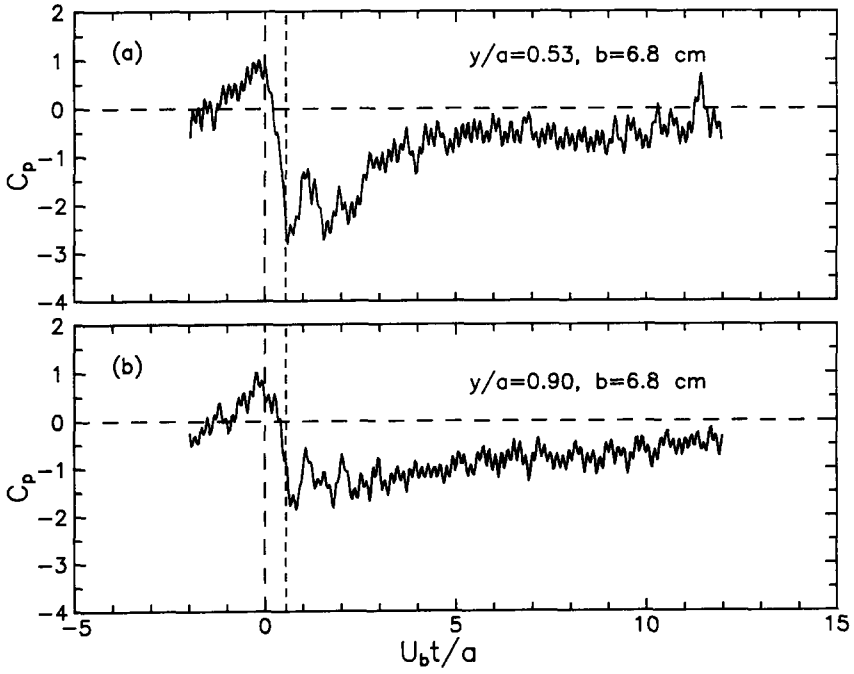

Figure 4. Pressure signals for the probe cutting (a) across and (b) outside the vortex for 163 μm bed with particles entrained in the freeboard region

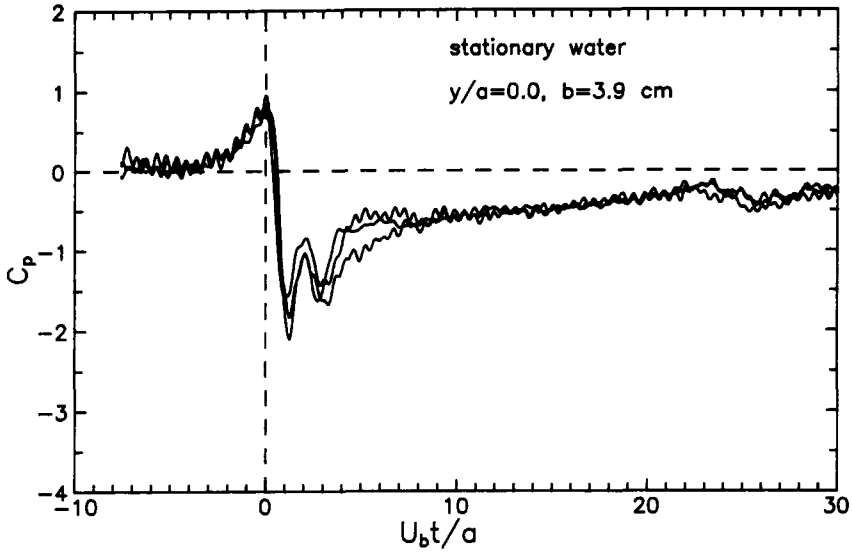

Figure 5. Pressure signals in stationary water along the bubble axis of symmetry for 3 experimental runs.

The signals shown in figure 5 are qualitatively similar to the results of Lazarek & Littman (1974) for stationary water. However, there are some important differences. In the present study, contrary to their work, the pressure traces obtained for different runs at the same location (y/a) are not identical, and pressure recovery is not complete after the primary wake. These differences can be attributed to the fact that in the study of Lazarek & Littman (1974), the wake is closed-laminar; this structure is invariant with time and secondary wake effects are negligible. The wakes observed in the present work are open with shedding vortices.

Typical signals in liquid–solid suspensions are shown in figure 6. These pressure distributions are qualitatively similar to those in water. Both the signals in figure 6 exhibit a second minimum and the concave region is relatively narrow. The pressure recovery is nearly complete, both signals indicating a smaller secondary wake compared with that of water.

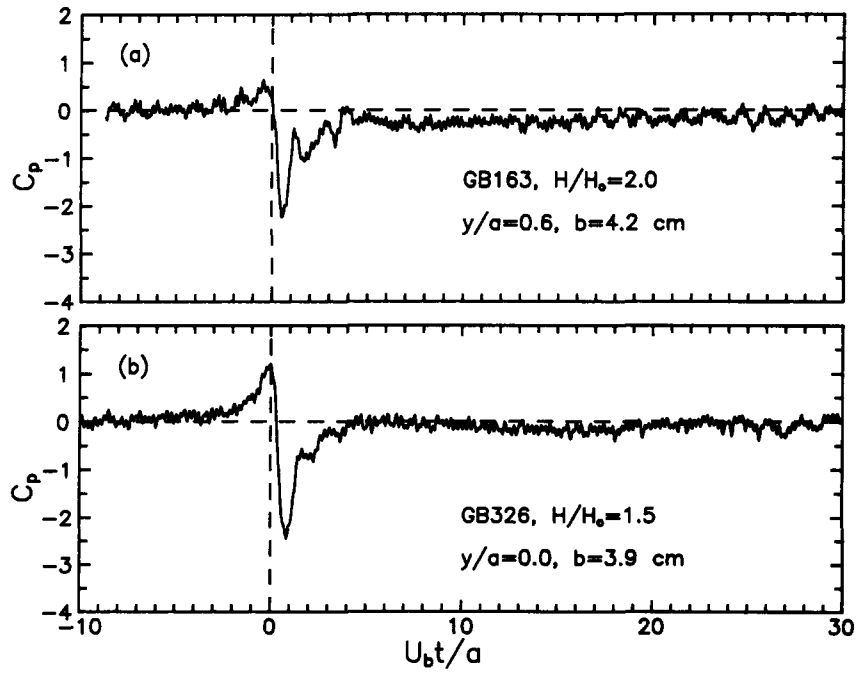

Figure 6. Comparison of typical pressure signals for GB326 and GB163.

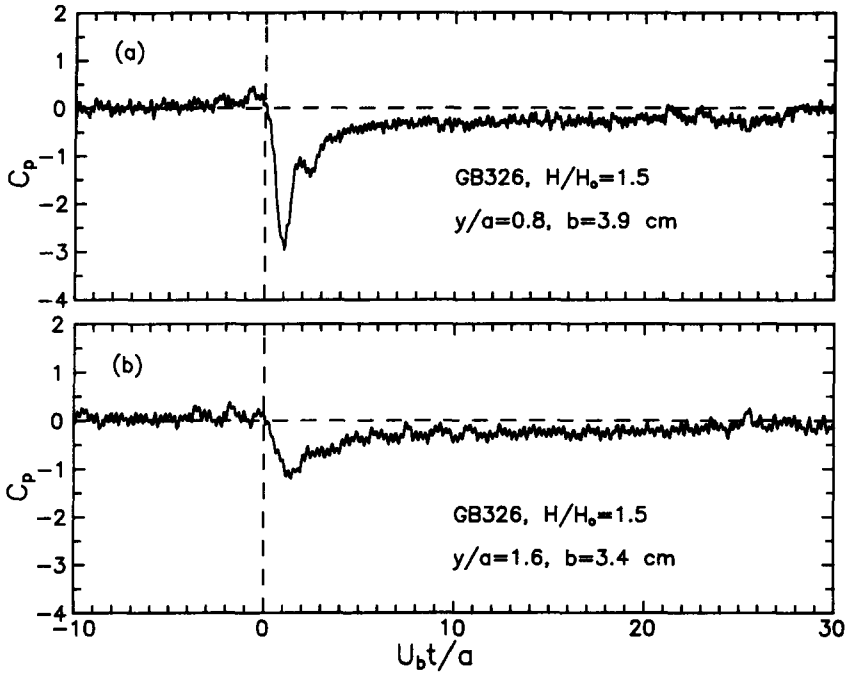

Figure 7. Typical pressure signal for a bubble hitting the probe at $y/a > 0$.

It should be noted that when the veritcal axis passing through the probe is away from the bubble axis of symmetry ($y/a > 0$), the first maximum occurs before the bubble nose reaches the horizontal plane of the probe. Typical signals for this case are shown in figure 7, figures 4(a, b) and 6(a) also represent this case. This is consistent with the isobaric representation of the frontal pressure field proposed by Lazarek & Littman (1974).

The size of the wake varies dynamically and its structure is dependent on a particular instant in the formation–growth–shedding cycle of vortices. Therefore, quantitative information regarding the wake parameters from the various pressure–time signals can be obtained by averaging their dynamic variations. As noted earlier (figure 3), for a given pressure trace, $(\tau_4 - \tau_2)$ gives an indication of the size of the vortex. The value of $(\tau_4 - \tau_1)$ corresponds to the size of the primary wake and $(\tau_2 - \tau_1)$ is for the stable liquid layer. It is easy to identify τ_1, τ_2 and τ_3 from a signal but τ_4 is difficult to identify when the probe lies outside the vortex boundary, as discussed earlier [figure 4(b)]. Hence it is assumed that the vortices are approximately symmetric about the horizontal plane passing through the vortex center. Thus, the average size of the vortex is given by $[2(\tau_3 - \tau_2)]$ and that of the primary wake becomes $[(\tau_2 - \tau_1) + 2(\tau_3 - \tau_2)]$. As the signals are dynamic in nature and vary with location, it is imperative to carry out the averaging over the entire lateral width of the bubble to draw any quantitative inferences. The averaging of the dynamic variation provides quantitative information about the sizes of the liquid wake, primary wake and vortex in stationary water, and liquid–solid beds with 163 and 326 μm glass beads (hereafter, the last two systems are referred to as GB163 and GB326, respectively). Table 2 shows the values of the quantities. Thus, the average size of the vortex is largest in stationary water. Also, the size of

Table 2. A measure of bubble-wake parameters over $y/a < 1$

System	Ave. liquid wake size[a]	Ave. vortex size[b]	Ave. primary wake size[c]	C_p at nose
Water	1.04	1.88	2.92	0.92
GB326 ($\epsilon_s = 0.32$)	1.06	1.65	2.71	1.28
GB326 ($\epsilon_s = 0.41$)	1.38	1.37	2.75	1.41
GB163 ($\epsilon_s = 0.32$)	0.65	0.98	1.63	0.87

[a] $(\tau_2 - \tau_1)$.
[b] $[2(\tau_3 - \tau_2)]$.
[c] $[(\tau_2 - \tau_1) + 2(\tau_3 - \tau_2)]$.

the vortex is larger for greater bed expansion. GB326 has a larger vortex compared with GB163. The average size of the primary wake, k_p, varies as $k_p(\text{water}) > k_p(\text{GB326}) > k_p(\text{GB163})$, indicating that the presence of particles dissipates the wake. However, the size of stable liquid layer is largest for GB326. The liquid wake in water is larger than that in GB163.

Bessler & Littman (1987) reported that for a viscous liquid the value of C_p at the bubble nose is < 1, as the present form of Bernoulli's theorem used for defining modified pressure coefficient C_p is based on inviscid flow. This is indeed the case for all the pressure signals for GB163 obtained in this work, and this is reflected in table 2. This suggests that the liquid–solid medium may be treated as a pseudo-homogenous mixture with a higher viscosity for GB163. However, for GB326 the value of C_p at the nose of the bubble is consistently > 1. This may be due to heterogeneous effects for the larger particle size, implying that the liquid–solid medium for this case cannot be treated as pseudo-homogeneous.

With increasing viscosity, the energy dissipation in the free shear layer increases. This causes the free shear layer to grow at a faster rate, effectively reducing the vortex size. A decrease in vortex size with increasing viscosity was also observed by Bessler & Littman (1987). Thus, as shown in table 2, due to the pseudo-homogeneous behavior of GB163, the vortex size is smaller compared with that in water. On the other hand, the heterogeneous effects caused by GB326 in the liquid–solid system destroy the ordered motion/circulation, again resulting in a smaller vortex size compared with that in water.

The results shown in table 2 also indicate that the average size of the stable liquid layer increases with increasing solids holdup for GB326. Around the wake central axis, the particles are propelled upward by the vortical flow towards the base of the bubble. At higher solids holdup, the heterogeneous effects in GB326, i.e. small-scale disturbances caused by random motion of solid particles and by the wakes of the individual particles, reduce the apparent strength of the vortical flow (Fan & Tsuchiya, 1990). Thus, fewer particles can approach the bubble base, resulting in an increase in the thickness of the stable liquid layer.

CONCLUDING REMARKS

The geometry of the primary wake is uniquely characterized by the pressure trace, and a one-to-one correspondence between the pressure distribution and vortical structure is established as follows:

(1) the first minimum in the pressure signal lies within the stable liquid layer;
(2) the second maximum is at the boundary between the stable liquid layer and the vortex;
(3) the second minimum occurs at the same horizontal level as the vortex center;
(4) the point (τ_4, C_{p4}), which is the end of the concave region and where the pressure signal begins to level off, corresponds to the cut-off stream at the lower end of the vortex.

The presence of solids has a significant effect on the primary wake parameters. GB326 exhibits noticeable heterogeneous effects, while GB163 resembles a homogeneous medium of a higher viscosity than pure water.

Acknowledgements—The authors thank Dr K. Tsuchiya for his valuable comments and suggestions. This work was supported by NSF Grant CTS-895463.

REFERENCES

BESSLER, W. F. & LITTMAN, H. 1987 Experimental studies of wakes behind circularly capped bubbles. *J. Fluid. Mech.* **185,** 137–151.

EL-TEMTAMY, S. A. & EPSTEIN, N. 1980 Rise velocities of large single two-dimensional and three-dimensional gas bubbles in liquids and in liquid fluidized beds. *Chem. Engng J.* **19,** 153–156.

FAN, L.-S. & TSUCHIYA, K. 1990 *Bubble Wake Dynamics in Liquids and Liquid–Solid Suspensions,* 1st edn. Butterworths, Stoneham, MA.

LAZAREK, G. M. & LITTMAN, H. 1974 The pressure field due to a large circular capped air bubble rising in water. *J. Fluid Mech.* **66,** 673–687.

TSUCHIYA, K. & FAN, L.-S. 1988 Near-wake structure of a single gas bubble in a two-dimensional liquid–solid fluidized bed: vortex shedding and wake size variation. *Chem. Engng Sci.* **43,** 1167–1181.